Phase-Locking Transition in a Chirped Superconducting Josephson Resonator

O. Naaman,[1] J. Aumentado,[2] L. Friedland,[3] J. S. Wurtele,[4,5] and I. Siddiqi[1]

[1]*Quantum Nanoelectronics Laboratory, Department of Physics, University of California, Berkeley, California 94720, USA*
[2]*National Institute of Standards and Technology, 325 Broadway, Boulder, Colorado 80305, USA*
[3]*Racah Institute of Physics, Hebrew University, Jerusalem 91904, Israel*
[4]*Department of Physics, University of California, Berkeley, California 94720, USA*
[5]*Center for Beam Physics, Lawrence Berkeley National Laboratory, Berkeley, California 94720, USA*

(Received 5 June 2008; published 12 September 2008)

We observe a sharp threshold for dynamic phase locking in a high-Q transmission line resonator embedded with a Josephson tunnel junction, and driven with a purely ac, chirped microwave signal. When the drive amplitude is below a critical value, which depends on the chirp rate and is sensitive to the junction critical current I_0, the resonator is only excited near its linear resonance frequency. For a larger amplitude, the resonator phase locks to the chirped drive and its amplitude grows until a deterministic maximum is reached. Near threshold, the oscillator evolves smoothly in one of two diverging trajectories, providing a way to discriminate small changes in I_0 with a nonswitching detector, with potential applications in quantum state measurement.

DOI: 10.1103/PhysRevLett.101.117005 PACS numbers: 85.25.Cp, 03.67.Lx, 05.45.−a, 74.50.+r

A superconductor-insulator-superconductor tunnel junction is a unique electrical circuit element that can be simultaneously nonlinear and nondissipative. The Josephson equations parametrize the nonlinear tunnel current $I = I_0 \sin\delta$ and voltage $V_J = \hbar\dot{\delta}/2e$ in terms of the gauge-invariant superconducting phase difference δ across the junction and its time derivative $\dot{\delta}$. These equations describe a nonlinear inductor with inductance $L_J(\delta) = \hbar/(2eI_0\cos\delta)$, which can be shunted with a low-loss reactance [1] to form a high quality-factor (Q) anharmonic oscillator. Coupling this Josephson oscillator to a quantum bit (qubit) produces a state dependent shift of the resonant frequency, thus realizing a dispersive measurement [2–4]. When probed with a small number of photons, the Josephson oscillator is essentially harmonic and the measurement does not project the quantum state out of the qubit basis: it can, in principle, be quantum nondemolition, and has a well characterized minimal backaction [5–9]. When driven more strongly, anharmonicity causes the resonant frequency to vary with the amplitude of oscillation [10], enhancing the oscillator's driven response to a frequency shift and the predicted measurement contrast in qubit readout. Moreover, the Josephson oscillator can also bifurcate [11] into two metastable oscillation states, resulting in a projective measurement. This has been demonstrated with the Josephson bifurcation amplifier [12] in which the oscillator is probed with a fixed frequency drive of varying amplitude [13,14]. The dynamical state of the oscillator depends on the qubit state, and measurement sensitivity arises from a sharp threshold for switching between the two dynamical states. While such a nonlinear oscillator has the advantage of measurement gain, the precise nature of its backaction on the quantum system, especially that associated with the switching process, and the degree to which a quantum nondemolition measurement is possible is still being investigated [15,16].

In this Letter, we demonstrate a measurement scheme that still drives the Josephson oscillator to the bifurcation regime but does not involve any switching process. Instead of applying an amplitude modulated drive, we apply a chirped microwave frequency drive to access a phenomenon known as autoresonance [17]. In response to frequency modulation, the oscillator may either phase lock to the chirped carrier and latch to a high-amplitude oscillation state or not lock to the drive and remain in a small-oscillation state. These two outcomes, which can be used as pointers for the state of a qubit, are separated in parameter space by a sharp threshold [18] that scales with the chirp rate and is sensitive to the junction I_0. Throughout its evolution, the oscillator tracks a single basin of attraction—no switching occurs, thus avoiding any potential backaction associated with switching dynamics and transient oscillations. We call this measurement device a Josephson chirped amplifier (JCA). We show that the observed threshold behavior is in excellent agreement with both analytic theory and numerical simulations, and estimate the possible contrast of the JCA in quantum state readout.

In our experiment, the Josephson oscillator was formed by an $Al/AlO_x/Al$ Josephson tunnel junction [Fig. 1(c)] placed in the middle of a high-Q niobium half wave coplanar waveguide resonator, with a characteristic impedance $Z_0 = 50\ \Omega$, and symmetrically coupled to the 50 Ω environment via capacitors $C_c \approx 10$ fF. The measurements were performed in a dilution refrigerator at $T = 20$ mK; the experimental setup is shown schematically in Fig. 1(a). Microwave excitation was applied to the resonator using an HP8780A vector signal generator, frequency

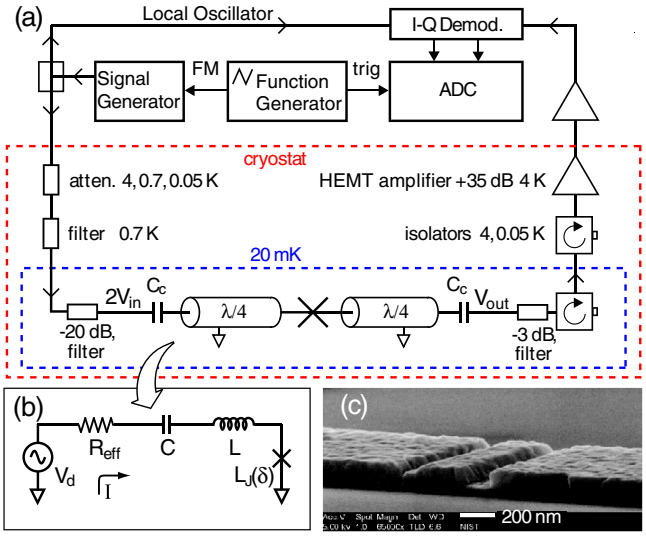

FIG. 1 (color online). (a) Schematic of the experimental setup. Input microwave lines are attenuated and filtered at the indicated temperature stages of the cryostat. Isolators provide a total of 80 dB isolation in the relevant frequency band. (b) Series *RLC* model of the resonator. (c) Scanning electron micrograph of the junction.

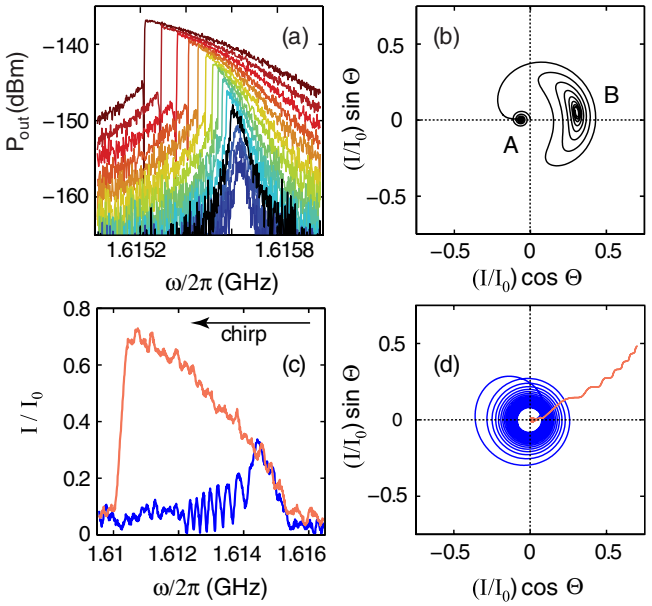

FIG. 2 (color online). (a) Transmitted power P_{out} in steady state, measured with a network analyzer. Input powers are -155.5 to -123 dBm at 2.5 dB step. (b) Simulated in-phase and quadrature components of current oscillations for detuning $(\omega - \omega_0)/2\pi = 0.5$ MHz and drive power ramped in time from -126 to -120 dBm. *A* and *B* label the low- and high-amplitude attractors, and Θ is the phase mismatch. (c) Response of the resonator to a chirped drive, $\alpha/2\pi = 5 \times 10^{11}$ Hz/s, at $P_{\text{in}} = -126$ dBm (blue, dark) and -120 dBm (red, light). (d) Simulated quadratures of the current in a chirped resonator with the same parameters as the data in (c). The simulation was terminated at $\omega/2\pi = 1.6106$ GHz.

modulated with a triangle waveform to provide a linear, phase-continuous frequency chirp with a 50 MHz span. Typical chirp rates, $\alpha = -d\omega/dt$, ranged from $\alpha/2\pi = 10^{11}$ to 10^{13} Hz/s. The transmitted microwave signal, V_{out}, was amplified and then demodulated (1.9 MHz IF bandwidth) to find its amplitude and phase. The amplitude of current oscillations in the resonator is given by $I = (2|V_{\text{out}}|/Z_0)\sqrt{Q/\pi}$.

We first measure the oscillator in steady state [Fig. 2(a)]. From the microwave transmission, P_{out}, at low power in the linear regime we measure $\omega_0/2\pi = 1.615\,64$ GHz and infer a quality factor $Q = 27\,500 \pm 1000$. The Q is limited by coupling to the 50 Ω environment and is within 10% of its predicted value $Q = \pi/4Z_0^2\omega_0^2C_c^2$. When the drive power exceeds a critical value $P_c = -148$ dBm, the oscillator response bifurcates into two branches [11]. From the measured P_c we estimate the junction critical current $I_0 = 0.61 \pm 0.04$ μA; this value is consistent with room temperature dc resistance measurements on cofabricated junctions. The stated uncertainties are dominated by cryogenic variations in the attenuation of the coaxial lines attached to the resonator. Additionally, the observed power at which bifurcation occurs at different drive frequencies agrees well with theory [1] using the measured values of P_c and Q.

Having characterized its parameters, we proceed to excite the oscillator with a chirped microwave drive. Figure 2(c) shows the resonator response to a downwards frequency chirp at the rate of $\alpha/2\pi = 5 \times 10^{11}$ Hz/s. At low power the amplitude of oscillations initially increases as the chirp passes through ω_0. However, as the chirp progresses towards lower frequencies, the resonator decouples from the drive and rings down to rest. For a stronger drive amplitude the response of the resonator changes dramatically: as the chirp passes through ω_0, the resonator phase becomes locked to the drive and its amplitude grows with time. A threshold for phase locking can be seen in Fig. 3, which shows the normalized amplitude of current oscillations, I/I_0, as a function of frequency and drive power for a fixed chirp rate. In region 1, at low powers, no phase locking is observed and the junction current grows only in the vicinity of ω_0. Above a critical drive power, P_c in Fig. 3, the resonator remains phase locked and its amplitude continues to grow up to a deterministic maximum, set either by damping (region 2) or by I_0 (region 3). The existence of a threshold for phase locking, which obeys a universal scaling law, was first observed in the context of non-neutral plasmas [19]; our work is the first observation of this transition in a microelectronic circuit operating at GHz frequency and mK temperature—5 orders of magnitude higher in frequency and lower in temperature than Ref. [19].

We proceed to briefly analyze the threshold phenomenon (a detailed analysis will be given elsewhere). The dynamics of a Josephson junction, ac biased through a resonant cavity near its resonance, can be modeled by the equivalent series *RLC* circuit shown in Fig. 1(b) [1,20],

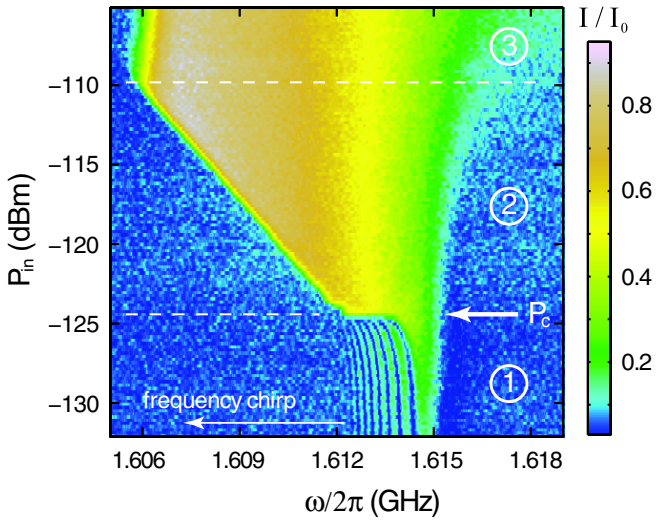

FIG. 3 (color online). Normalized amplitude of current oscillations in the resonator as a function of drive power and frequency, with the frequency swept downwards at a rate of 5×10^{11} Hz/s. The arrow indicates the critical power P_c for phase locking.

where $\tilde{L} \equiv L + L_J(0) \approx \pi Z_0/2\omega_0 = 7.74$ nH, $C \approx 2/\pi Z_0 \omega_0 = 1.25$ pF, and $\omega_0^2 = 1/\tilde{L}C$. The effective loss due to external loading is $R_{\rm eff} = \pi Z_0/2Q$, and the effective drive amplitude is $V_d = V_{\rm in}\sqrt{\pi/Q}$ where $V_{\rm in} = \sqrt{2Z_0 P_{\rm in}}$ is the amplitude of the incident wave referred to a matched load. From Kirchoff's voltage law we obtain an equation of motion for the charge $\tilde{q}(t) = \int I(t')dt'$ in the circuit. Defining the nonlinearity ratio $2a = L_J(0)/\tilde{L}$, and the dimensionless time $\tau = \omega_0 t$, charge $q = (\omega_0\sqrt{2a}/I_0)\tilde{q}$, and drive $\epsilon = (\sqrt{2a}/\tilde{L}I_0\omega_0)V_d$, and expanding the voltage drop across the junction to second order in I/I_0, the equation of motion in the weakly nonlinear regime [19] becomes

$$\ddot{q}(1 + \dot{q}^2/2) + q + \nu\dot{q} = \epsilon\cos\phi_d, \tag{1}$$

where $\nu = 1/Q$, $\phi_d = \omega_0 t - \alpha t^2/2$ is the phase of the chirped drive, and the derivatives are with respect to τ.

Transforming to a chirped frame rotating with the drive [where Eq. (1) reduces to the Duffing model [1]], and neglecting fast oscillating terms, we cast Eq. (1) into an equation for the complex variable $\Psi = A\exp(i\Theta)$, where A is proportional to the amplitude of $q(\tau)$, and Θ is the phase mismatch between $q(\tau)$ and the drive:

$$i\frac{d\Psi}{d\tilde{\tau}} + (|\Psi|^2 - \tilde{\tau} + i\gamma/2)\Psi = \mu. \tag{2}$$

Here $\tilde{\tau} = \alpha^{1/2}\tau/\omega_0$, $\gamma = \omega_0\alpha^{-1/2}/Q$, and $\mu = \epsilon\omega_0^{3/2}\alpha^{-3/4}/8$. Equation (2), with the initial condition $\Psi = 0$ at $\tilde{\tau} \to -\infty$, admits two asymptotic solutions at $\tilde{\tau} \to +\infty$: a solution decoupled from the drive for $\mu < \mu_{\rm cr}$, in which Θ grows quadratically with time, and a phase-locked solution, $\Theta = {\rm const}$, for $\mu > \mu_{\rm cr}$.

In the absence of damping [21] the transition between the two solutions of Eq. (2) occurs for $\mu_{\rm cr}^0 = 0.41$. When damping is present, $\mu_{\rm cr}$ increases and becomes dependent on the damping: $\mu_{\rm cr}(\gamma) \simeq \mu_{\rm cr}^0(1 + a\gamma + b\gamma^2)$ for $\gamma \ll 1$, with coefficients $a = 1.06$ and $b = 0.67$ found numerically.

Combining the definitions above for μ and ϵ, we find the critical drive amplitude for phase locking:

$$V_d^{\rm cr} = 8\sqrt{\frac{2e}{\hbar\omega_0}}(\tilde{L}I_0)^{3/2}\alpha^{3/4}\mu_{\rm cr}. \tag{3}$$

The scaling law $V_d^{\rm cr} \propto \alpha^{3/4}$ is exact only in a lossless resonator. For finite dissipation, $\gamma \propto \alpha^{-1/2}$ and corrections to this law enter through $\mu_{\rm cr}(\gamma)$.

To compare the observed value of the phase-locking threshold, $V_d^{\rm cr}$, to the theory outlined above, we first note that the probability of phase locking, $P_{\rm lock}$, obtained from averaging the response from 5000 frequency sweeps, grows from zero to one over a finite range of drive amplitudes. A typical phase-locking probability "s curve" is plotted in the inset of Fig. 4 as a function of V_d for $\alpha/2\pi = 2 \times 10^{12}$ Hz/s, where we define the threshold at $P_{\rm lock} = 0.5$. We measured $V_d^{\rm cr}$ as a function of chirp rate, and the results are plotted in Fig. 4 (□). We also performed numerical simulations of the fully nonlinear equation of motion for $\tilde{q}(t)$ in the series RLC model of Fig. 1(b), without further approximations, and using experimentally determined parameters. We simulated both a resonator with $Q = 27\,500$ and a lossless one. The results of the

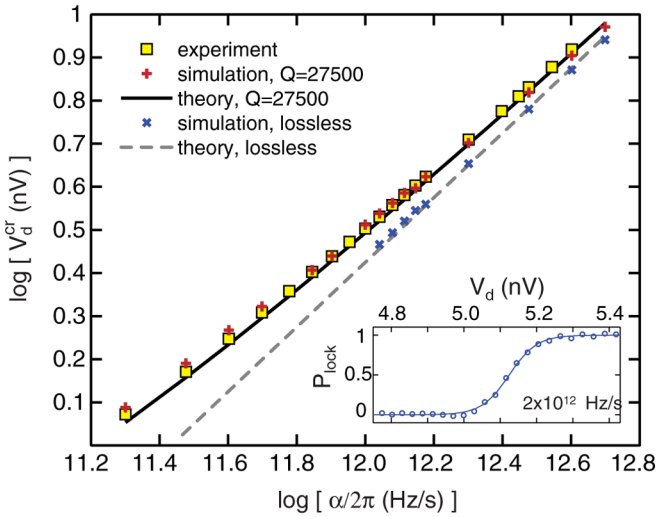

FIG. 4 (color online). Comparison of the experimental (□) critical drive voltage versus chirp rate to Eq. (3), with (solid line) and without (dashed line) dissipation. Also shown are values for the critical drive from simulations of the fully nonlinear equation of motion for the equivalent RLC circuit, for a lossless resonator (×) and for $Q = 27500$ (+). Inset: Probability of phase locking versus drive amplitudes near threshold at $\alpha/2\pi = 2 \times 10^{12}$ Hz/s, evaluated over a 0.5 MHz frequency band centered at 1.6095 GHz. Solid line is a sigmoidal fit.

simulations and the predictions from Eq. (3) with (solid line) and without (dashed line) damping are also plotted in Fig. 4. We observe excellent agreement between experiment and theory if damping is included. Note that this is not a fit—all parameters are fixed to their experimentally determined values. Moreover, the agreement of Eq. (3) with the fully nonlinear simulations confirms the validity of the weak nonlinearity assumptions made in the threshold analysis, and reflects the result that phase locking occurs at small oscillation amplitudes [17].

From the measured width of the phase-locking threshold we can estimate the potential sensitivity of the JCA, where as a benchmark we consider detecting a 1% variation in I_0, a typical signal associated with the transition between the ground and excited state of a superconducting ''quantronium'' qubit [22]. The discrimination power of the device can be estimated from the fractional change in critical current, $\Delta I_0/I_0$, that will shift the ''s curve'' by an amount equal to the threshold width: $\Delta I_0/I_0 \simeq 2\Delta V_d^{\mathrm{cr}}/3V_d^{\mathrm{cr}}$ from Eq. (3). For the data in the inset of Fig. 4, and defining the width ΔV_d^{cr} for $0.27 < P_{\mathrm{lock}} < 0.73$, we find $\Delta I_0/I_0 = 9.6 \times 10^{-3}$. The 1% variation in I_0 (6.1 nA for our device) can be resolved with ~46% contrast; the ultimate sensitivity of the JCA requires an understanding of the dependence of the threshold width on noise, both classical and quantum. For this chirp rate of 2×10^{12} Hz/s, a single measurement can be accomplished in less than 10 μs. Significantly faster chirp rates and shorter measurement times are in principle possible.

The dynamics associated with operating the amplifier with a frequency-modulated (FM) drive versus an amplitude-modulated (AM) drive are quite different. In Figs. 2(b) and 2(d) we show the calculated in-phase and quadrature phase components of I/I_0 for AM and FM drives, respectively. In the AM case, for detuning $\omega < \omega_0$, the system can switch from a low-amplitude oscillation attractor (A) to a high-amplitude oscillation one (B), with significant phase oscillations associated with the switching as shown in Fig. 2(b). In contrast, the trajectories shown in Fig. 2(d) for a chirped drive indicate that the system smoothly tracks the evolution of the high-amplitude attractor without spurious oscillations of the phase. Another feature of the JCA is that we can potentially perform quantum measurement with very few photons (near ω_0), but ''latch'' and record the signal with a large number of photons at a final frequency $\omega < \omega_0$, so that minimal fidelity is lost due to noise in the measurement electronics.

In summary, we have observed that a high-Q resonator embedding a Josephson junction subject to a chirped drive exhibits a transition to phase locking with a sharp threshold that can be used for detecting small changes in I_0. This device—the Josephson chirped amplifier—provides a new route for nonlinear, dispersive quantum measurement, and a test bed for nonequilibrium quantum statistical mechanics in a rotating frame with time-dependent frequency. We studied the dependence of the critical drive on the chirp rate and found excellent agreement with both theory and simulations. The phase-locked, highly excited state, and the associated phase-locking threshold are a robust feature of chirped nonlinear oscillators, and should be observable in any system with low loss and weak nonlinearity: electrical, mechanical, or photonic, for example. Finally, we note that another approach to observing these phase-locking effects is to modulate the resonant frequency of the oscillator in the presence of a harmonic drive; a candidate technology for such tuning was recently demonstrated in Ref. [23] in the context of variable coupling elements for qubits.

The authors thank R. Vijayaraghavan, V. Manucharyan, and J. Clarke for useful discussions. Financial support was provided by the Office of Naval Research under Grant No. N00014-07-1-0774 (O. N., I. S.), UC Berkeley Chancellor's Faculty Partnership Fund (I. S.), the Hellman Family Faculty Fund (I. S.), the U.S.-Israel Binational Science Foundation under Grant No. 2004033 (L. F., J. W.), and the U.S. Department of Energy under Grant No. DE-FG02-04ER41289 (J. W.).

[1] V. E. Manucharyan *et al.*, Phys. Rev. B **76**, 014524 (2007).
[2] E. Il'ichev *et al.*, Phys. Rev. Lett. **91**, 097906 (2003).
[3] A. Lupaşcu *et al.*, Phys. Rev. Lett. **93**, 177006 (2004).
[4] A. Wallraff *et al.*, Nature (London) **431**, 162 (2004).
[5] H. J. Kimble, Phys. Scr. **T76**, 127 (1998).
[6] P. Grangier, J. A. Levenson, and J. P. Poziat, Nature (London) **396**, 537 (1998).
[7] A. Blais *et al.*, Phys. Rev. A **69**, 062320 (2004).
[8] D. I. Schuster *et al.*, Phys. Rev. Lett. **94**, 123602 (2005).
[9] M. Boissonneault, J. M. Gambetta, and A. Blais, Phys. Rev. A **77**, 060305 (2008).
[10] L. D. Landau and E. M. Lifshitz, *Mechanics* (Butterworth-Heinemann, Oxford, 2001).
[11] I. Siddiqi *et al.*, Phys. Rev. Lett. **94**, 027005 (2005).
[12] I. Siddiqi *et al.*, Phys. Rev. Lett. **93**, 207002 (2004).
[13] I. Siddiqi *et al.*, Phys. Rev. B **73**, 054510 (2006).
[14] A. Lupaşcu *et al.*, Phys. Rev. Lett. **96**, 127003 (2006).
[15] N. Boulant *et al.*, Phys. Rev. B **76**, 014525 (2007).
[16] A. Lupaşcu *et al.*, Nature Phys. **3**, 119 (2007).
[17] J. Fajans and L. Friedland, Am. J. Phys. **69**, 1096 (2001).
[18] J. Fajans, E. Gilson, and L. Friedland, Phys. Plasmas **6**, 4497 (1999).
[19] J. Fajans, E. Gilson, and L. Friedland, Phys. Rev. Lett. **82**, 4444 (1999).
[20] E. Boaknin *et al.*, arXiv:cond-mat/0702445.
[21] E. Grosfeld and L. Friedland, Phys. Rev. E **65**, 046230 (2002).
[22] M. Metcalfe *et al.*, Phys. Rev. B **76**, 174516 (2007).
[23] M. Sandberg *et al.*, Appl. Phys. Lett. **92**, 203501 (2008).